Supplementary Information

Hot Spot-Localized Artificial Antibodies for Label-Free Plasmonic Biosensing

Abdennour Abbas[1], Limei Tian[1], Jeremiah J. Morrissey[2,3] Evan D. Kharasch[2,3,4] and Srikanth Singamaneni[1,3]*

[1]*Department of Mechanical Engineering and Materials Science. Washington University in St. Louis, St Louis, MO, 63130, USA.*
[2]*Department of Anesthesiology, Division of Clinical and Translational Research, Washington University in St. Louis, St Louis, MO, 63110, USA*
[3] *Siteman Cancer Center*
[4]*Department of Biochemistry and Molecular Biophysics, Washington University in St. Louis, St Louis, MO, 63110 USA*

This file contains:

Figure S1

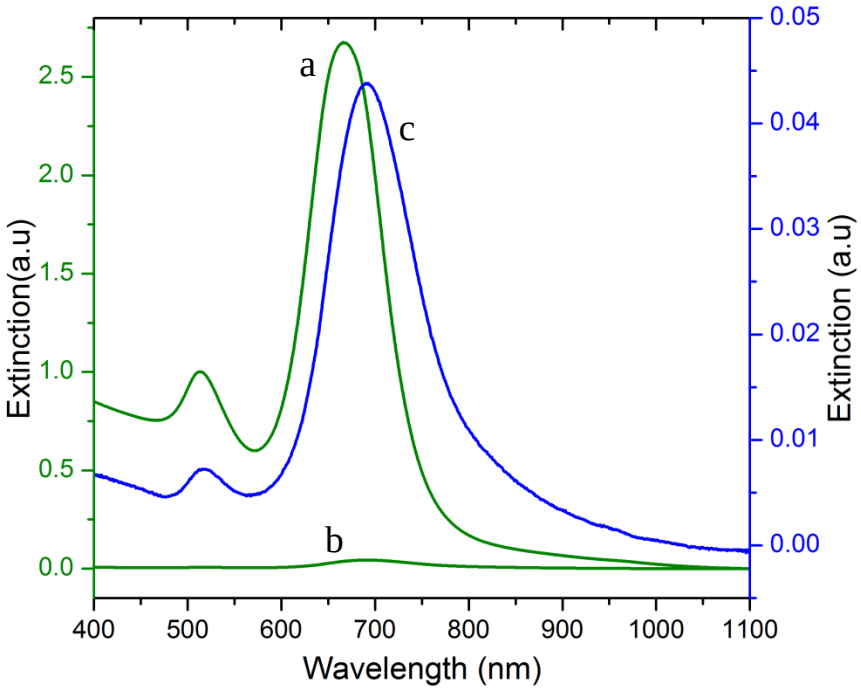

Figure S1: Figure S1: Extinction spectra of gold nanorods in (a) solution and on (b) glass substrates. For comparison purposes, the blue line (c) represents spectrum b with a different scale. The transfer of the nanorods from solution to a glass substrates results in a decrease of the extinction intensity by 10 to 50 times and a red-shift by ~30 nm. This shift is caused by the significant increase in refractive index in one side of the nanorods from n=1.33 (water) to n=1.5 (glass substrate).

Figure S2

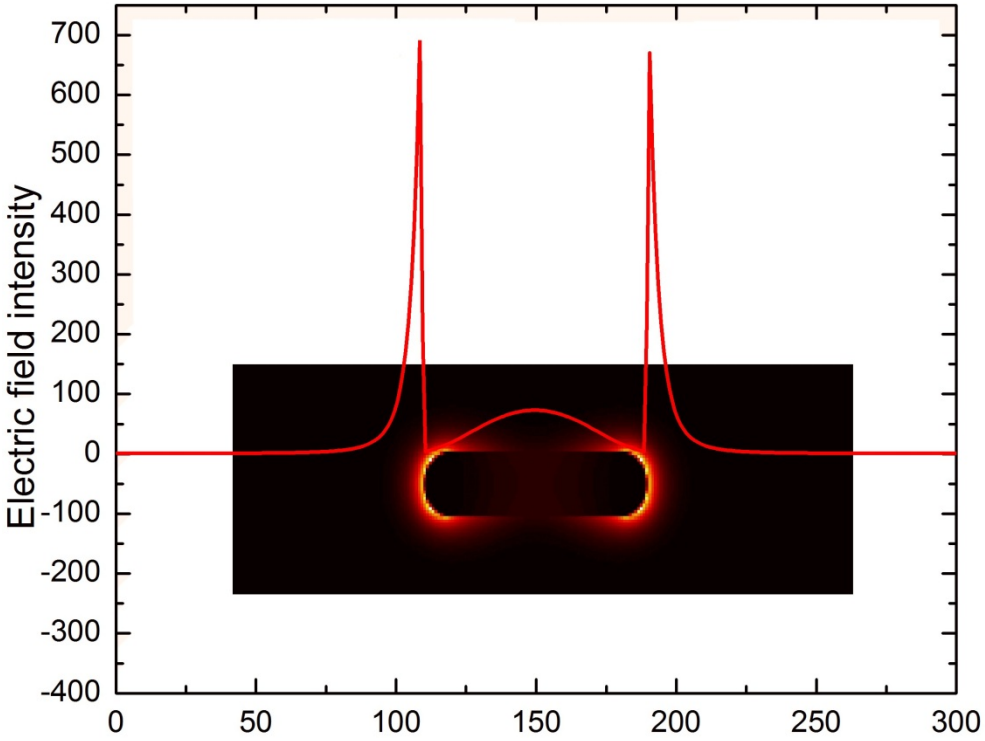

Figure S2. Profile and distribution of the electric field intensity around the gold nanorods. The intensity at the nanorods ends is one order of magnitude higher than that at the center of the nanorods. The intensity, however, decreases exponentially by increasing distance from the nanorods surface. The *x*-axis is in nm.

Figure S3

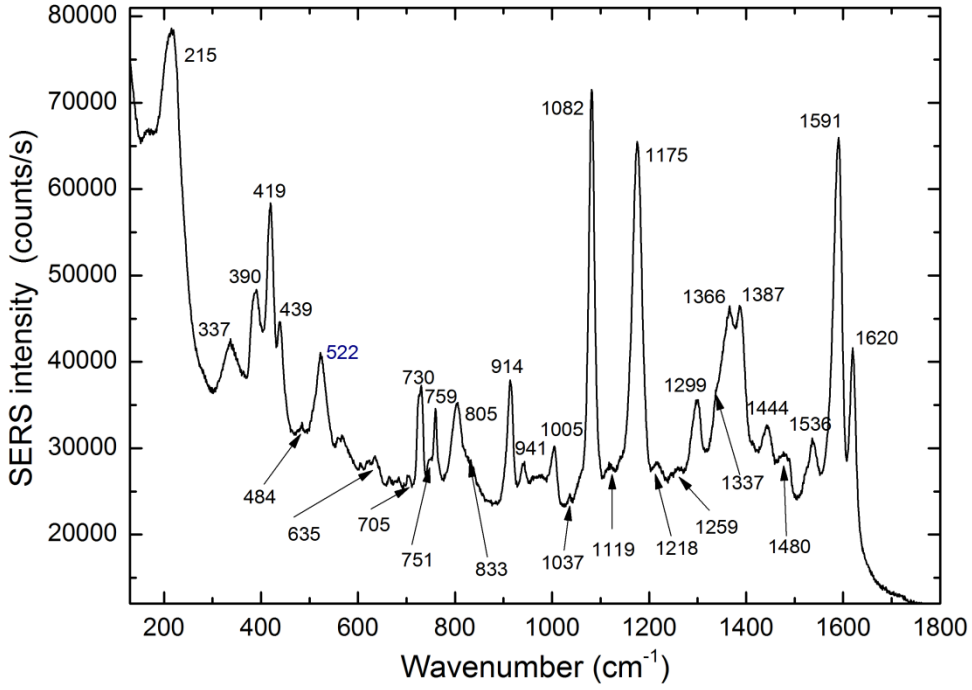

Figure S3. Surface enhanced Raman scattering of molecularly imprinted AuNRs after BSA protein capture. The assignments of the different bands are indicated in Table S1.

Figure S4

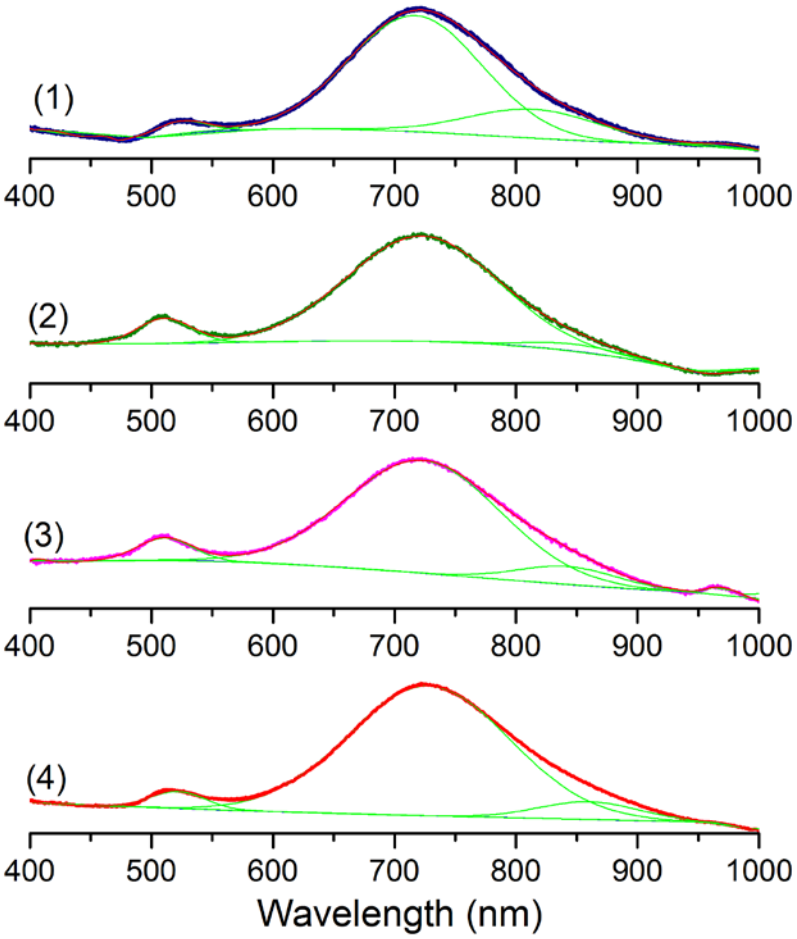

Figure S4. Template release using oxalic acid and SDS. Fitting of the extinction spectra provides the integrated surface area (A) of the peak due to the template fluorescein conjugated BSA at $\lambda \approx$ 500 nm. (1) AuNR before template immobilization (A= 4.28), (2) AuNR after template immobilization (A= 9.39), (3) template release using oxalic acid (A= 8.33), template release using a mixture of oxalic acid and SDS (A= 6.4).

Figure S5

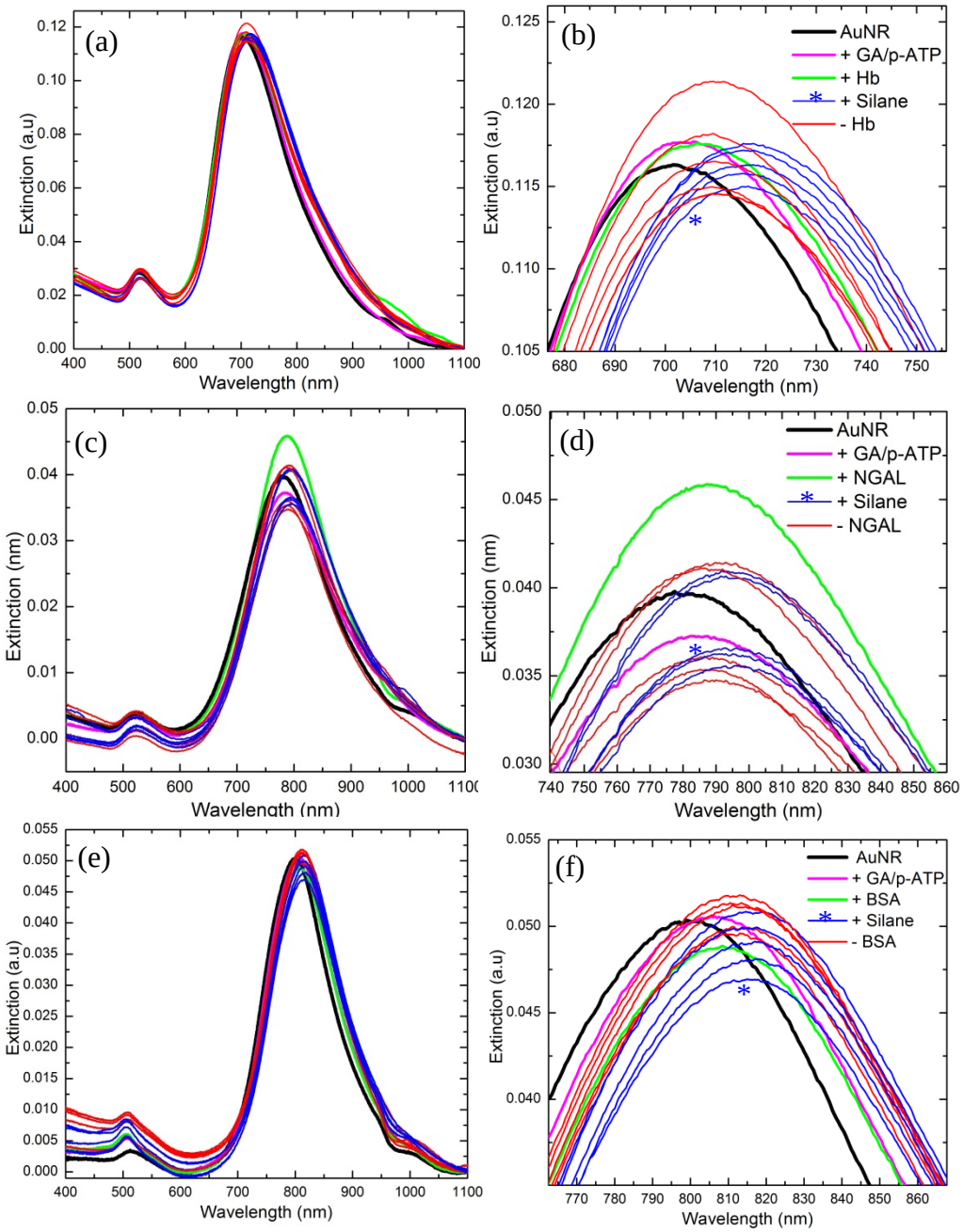

Figure S5. Extinction spectra of Hemoglobin (a, b), NGAL (c, d) and BSA (e, f) capture/release cycles with molecularly imprinted AuNRs. The spectra represent AuNRs (black line) before and after successive addition of glutaraldehyde/p-ATP (pink line), proteins (green line) and siloxane copolymers (blue line with a star). The red and blue lines represent different cycles of protein capture (blue) and release (red). These different steps and cycles correspond to the data plotted in Figure 5a.

Figure S6

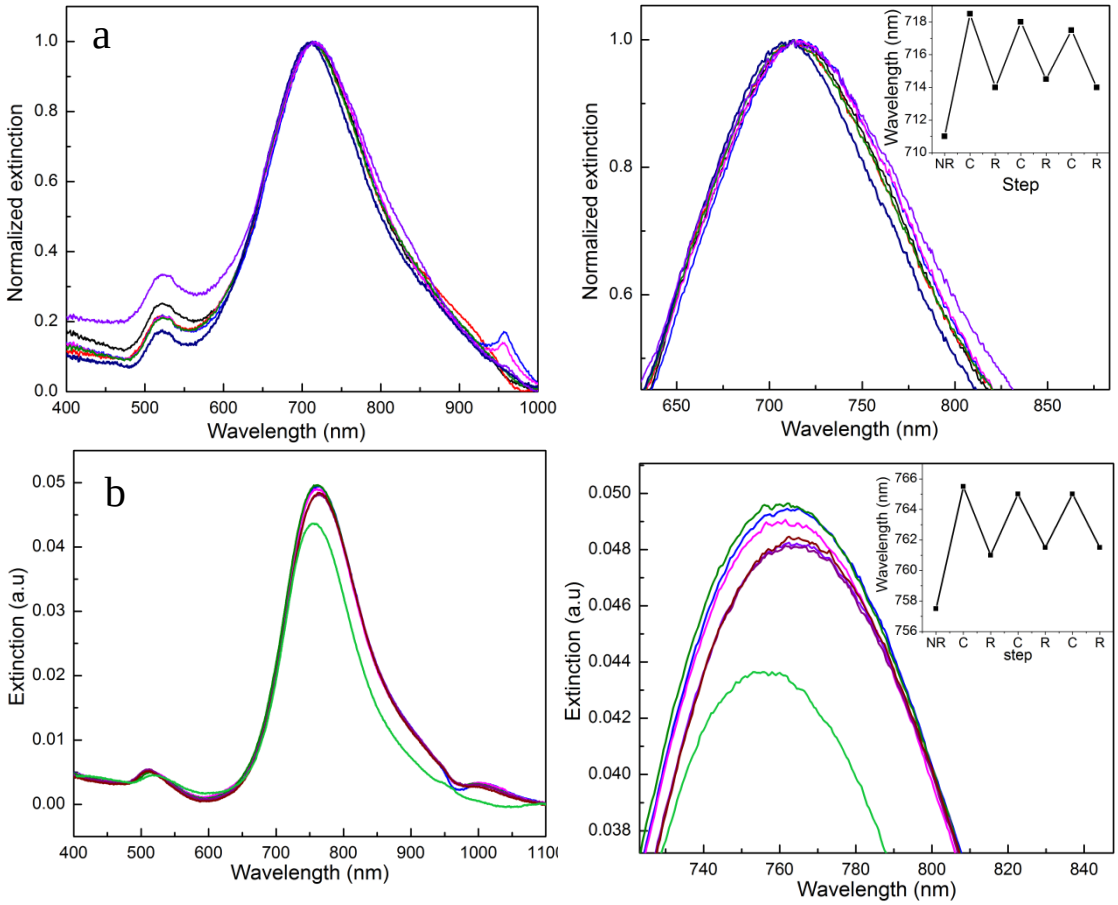

Figure S6. Extinction spectra of IgG (a) and allophycocyanin (b) capture/release cycles with molecularly imprinted AuNRs. The LSPR shifts are depicted in the insets. NR: imprinted nanorods, C: template capture, R: template release.

Figure S7

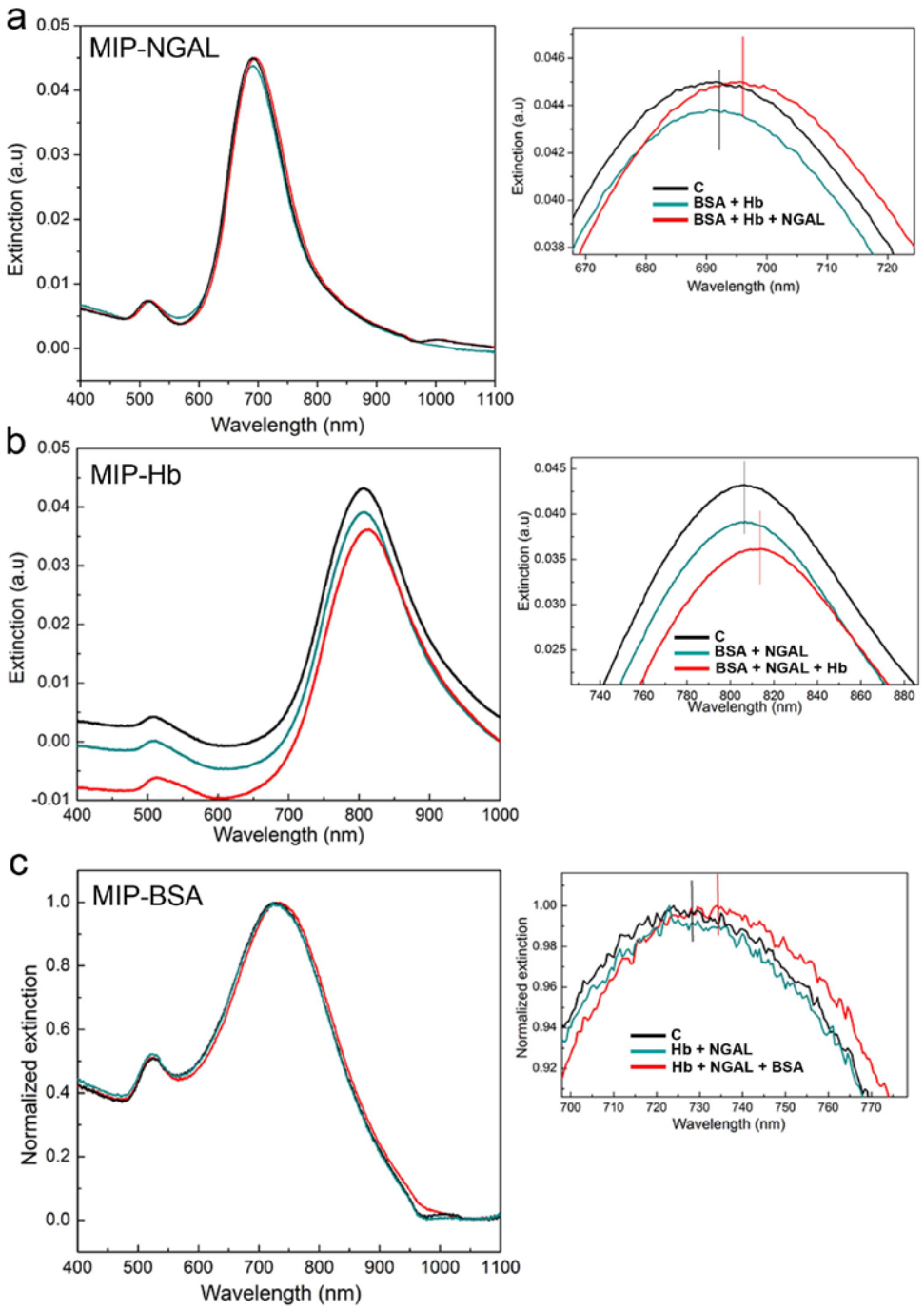

Figure S7. Localized surface plasmon resonance analysis of different protein mixtures using three different imprinted sensors with a specificity for (a) hemoglobin, (b) BSA and (c) NGAL proteins. The black line labelld C represents the extinction spectrum of the sensor after expositition to buffer. The green and red spectra are respectively obtained after exposition of the imprinted sensor to mixtures of two or three different proteins. A shift of 4-5 nm is observed only when the sensor is exposed to a mixture containing the protein used for imprinting (red line). The other spectra exhibit less than 1 nm LSPR shift.

Figure S8

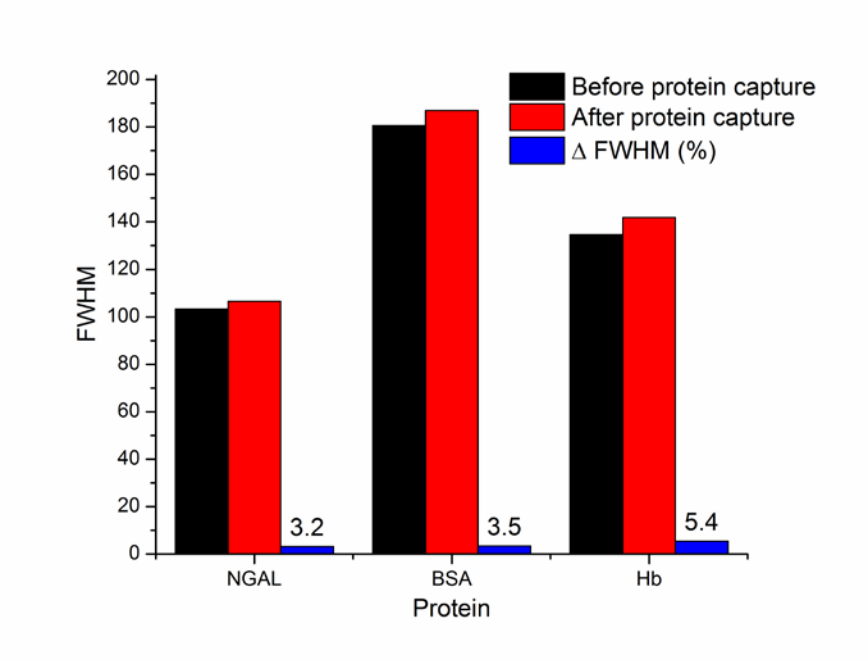

Figure S8. Change of the full width at half maximum (FWHM) of the extinction spectra before and after protein capture with the imprinted sensors. The data are obtained from the analysis of the spectra depicted in Figure S7. In all cases, the increase in FWHM (Δ FWHM) is lower than 10 %. This change seems to increase with increasing protein size but more investigation with a larger number of proteins is needed to understand the different contributions to the increase in FWHM.

Figure S9

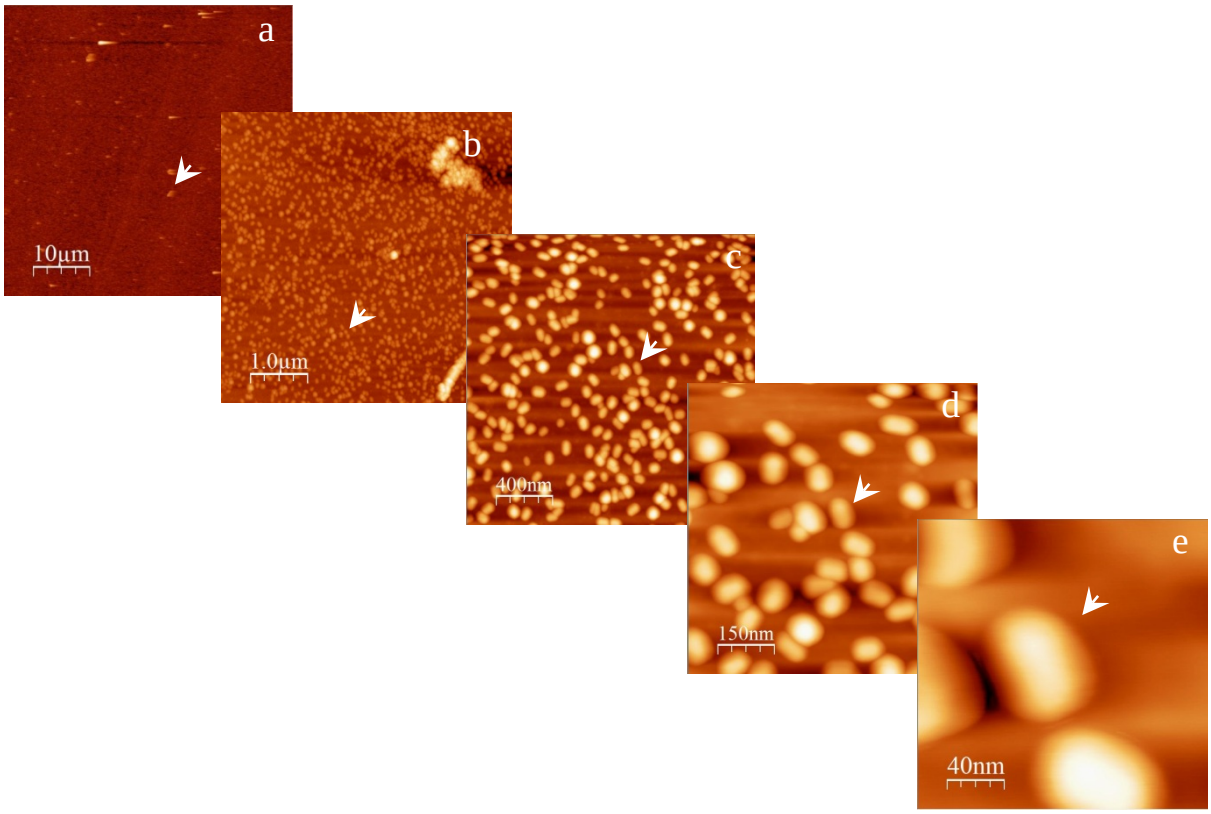

Figure S9: Atomic Force Microscopy (AFM) images depicting the multiple scan size used to localize and monitor thickness change of the MIP-AuNRs. The scan sizes are (a) 50 um x 50 um, (b) 5 um x 5 um, (c) 2 um x 2 um, (d) 760nm x 760 nm, (e) 368 nm x 368 nm.

Table S1. Selected SERS bands of CTAB, p-ATP and Proteins with their vibrational assignements*.

SERS band	***Vibrational Assignments***
CTAB	
752 m	CH_3 rock from $N^+(CH_3)_3$ group
760 w	CH_3 rock from $N^+(CH_3)_3$ group
956 w	CH_2 rock
1044 vw	CH_2 twist crystalline
1062 m	C-C sym stretch + CH_2 wag
1146 vw	C-C asym stretch + CH_2 wag
1292 m	CH_2 twist
1366 vw	C– CH_3 sym bending
1394 vw	C-H sym bend from $N(CH_3)_3$ group
1438 s	– CH_2 bend
1462 sh	– CH_2 bend
2844 s	C– H sym stretch of –CH_2 –
2876 vs	C– H sym stretch of –CH_3
2938 w	C– H asym stretch of –CH_2 –
p-ATP	
1083s	ν(CS)+ ρ (NH2)
1143 m	δ (CH)
1184 m	ν(CN) + ρ (CH)
1394 m	ν(CC) in Ph ring + ρ (CH) + ρ (NH2)
1439 m	ν(CC) in Ph ring + ρ (NH2)
1587 s	ν(CC) in Ph ring + δ (NH2)
Protein	
618 w	COOH bend
730 s	NH_2 bend
759	Au-S-C
962 m	ν (C-C)
1037 w	ν C-N
1119	ν C-N
1317 m	CH_2 wag
1462 w	CH_2 bend
1591 w	ν_{as} COOH
1005, 1037	Phe
845	Tyr
635, 705	ν C-S of cystein
522	ν S-S of disulfide bridges
1005	Symmetric benzene and purrole out-of-phase breathing mode of Trp, Phe
1366	Trp
1299	Alpha helix amide III
1165	Phe
1037	Phenyl
833	Tyr

*Table based on references: [S1-S6]

NGAL biomarker description

Neutrophil gelatinase-associated lipocalin (NGAL) is a member of the lipocalin family of proteins. Although originally linked to neutrophils in the blood, NGAL is also produced in small amounts by the normal kidney and excreted in the urine. In a wide variety of common kidney diseases, renal NGAL synthesis and excretion in the urine are increased almost 10-fold. During acute kidney injury, urinary NGAL levels are increased by several log-orders (100 to 1,000-fold) of magnitude. Additionally, plasma NGAL concentrations are increased during inflammation and neoplasia. Thus, measurement of plasma and urine NGAL levels is of clinical importance such that companies have marketed NGAL assays all of which are immune-based. Considering that about 13% of people in developing countries have some form of chronic kidney disease and that 15-30% of patients in any intensive care unit develop acute kidney injury during their hospital stay, there is a critical need for a low-cost, simple, stable and reliable NGAL assay. The above considerations clearly suggest the need for a label-free approach for rapid and quantitative detection of the proteins in urine at physiologically relevant concentrations (ng/ml).

Supporting References

[S1] K. Kalyanasundaram, J. K. Thomas, *J. Phys. Chem. A* **1976**, *80*, 1462.
[S2] R. Foucault, R. L. Birke, J. R. Lombardi, *Langmuir* **2003**, *19*, 8818.
[S3] M. Baia, F. Toderas, L. Baia, J. Popp, S. Astilean, *CPL* **2006**, *422*, 127.
[S4] A. Sabur, M. Havel, Y. Gogotsi, *J. Raman Spectrosc.* **2008**, *39*, 61.
[S5] R. A. Alvarez-Puebla, A. Agarwal, P. Manna, B. P. Khanal, P. Aldeanueva-Potel, E. Carbó-Argibay, N. Pazos-Pérez, L. Vigderman, E. R. Zubarev, N. A. Kotov, L. M. Liz-Marzán, *Proc. Natl. Acad. Sci. USA* **2011**, *108*, 8157.
[S6] M. Iosin, F. Toderas, P. L. Baldeck, S. Astilean, *J. Mol. Struct.* **2009**, *924-926*, 196.